Service Life Modeling of Reinforced High Volume Fly ash (HVFA) Concrete Structures Containing Cracks

Scott Z. Jones[a], Dale P. Bentz[a], Kenneth A. Snyder[a], Nicos S. Martys[a], Daniel S. Hussey[b], David L. Jacobson[b]

[a]*Engineering Laboratory, Materials and Structural Systems Division*
[b]*Physical Measurement Laboratory, Radiation Physics Division*
National Institute of Standards and Technology, 100 Bureau Dive, Gaithersburg, Maryland, 20899 USA

Abstract

Chloride ions, resulting from the application of de-icing salts, travel through the concrete matrix by diffusion in a connected pore network. Cracks in concrete facilitate chloride movement by allowing ions to bypass the concrete matrix and travel directly to reinforcing bars, reducing the protective capacity of the alkaline environment and the time to corrosion initiation. In this study, five concrete mixtures, two of which are high volume fly ash (HVFA) mixtures are investigated. Their diffusivity is assessed via electrical resistivity measurements and their chloride binding capacity is measured by submerging ground mortar specimens in a solution of NaCl. Neutron tomography of epoxy and methacrylate-filled cracks provides insights into the ability of concrete crack fillers to seal cracks. These results are incorporated into a service life model where the chloride ion concentration in a reinforced concrete slab is computed given a chloride ion exposure condition. The output of the model is the service life, defined to be the time required for the chloride concentration to reach a threshold level at the depth of the reinforcement. A service life model that incorporates diffusivity and chloride binding measurements, as well as capturing the effects of cracking, will improve service life predictions and help to determine the appropriate use of polymer crack fillers in reinforced concrete structures. Experimental and simulation results suggest that HVFA concretes can have longer service lives than their ordinary portland cement (OPC) concrete counterparts due to their decreased diffusivity and increased chloride binding. Crack fillers are able to fill moderate sized cracks and prevent chloride ion ingress, increasing the service life of the structure.

1. Introduction

Reinforced concrete structures exposed to northern climates, where de-icing salts are used during the winter months, are susceptible to steel reinforcement corrosion precipitated by the ingress of chloride ions into the concrete. Chloride ions traverse the pore structure of the concrete down to the rebar where they accumulate and depassivate the steel. Ordinary portland cement (OPC) concretes with a low water-to-cement ratio (*w*/*c*) have diffusivities sufficiently low to provide adequate protection from chloride ingress over the intended lifetime of the structure. The presences of cracks in the concrete, however, provide additional pathways for chloride ions to reach the rebar (Darwin et al., 2004; Lindquist et al., 2006), and can significantly reduce the service life of the concrete.

The current emphasis on concrete sustainability has renewed the interest in high volume fly ash (HVFA) concretes, which introduces new variables into service life prediction models (Bentz et al., 2013). Concrete mixtures containing fly ashes may have lower hydroxyl (OH^-) concentrations and, thereby, decrease the concentration of chlorides

necessary to initiate corrosion (Diamond, 1981). This paper seeks to address this concern and to expand on existing concrete service life models by implementing a model for chloride ingress into concrete derived from a mass balance on a differential concrete element. Five concrete mixtures, three OPC mixtures with various volume fractions of aggregates and two fly ash and limestone ternary mixtures, are made in the laboratory. For these mixtures, the diffusivity, chloride binding, and OH^- concentrations (within the pore solution) are measured. These results are used as inputs to a numerical model that predicts the free chloride ion concentration in the pore solution as a function of time and depth. The service life is calculated based on the ratio of $[Cl^-]$ to $[OH^-]$, and whether plain rebar, epoxy coated rebar, or a corrosion inhibitor is used. The simulations are repeated for the case of a crack in the concrete and when the crack is filled with methacrylate or epoxy. Results show the HVFA concretes created for this study have diffusivities lower than those of the OPC concretes for similar paste/aggregate volume fractions. Simulation results suggest a crack has a significant effect on service life, which can be effectively mitigated with crack fillers.

2. Materials and Methods

2.1 Concrete Mixture Proportions

Three OPC control mixtures with up to 75 % aggregate content and two fly ash and limestone concrete mixtures, one with an ASTM C618 class F fly ash and the other with a class C fly ash are studied. An ASTM C150 Type I cement from the Cement and Concrete Reference Laboratory (CCRL) is used for all concrete mixes, specifically CCRL cement 192. The oxide composition and other characteristics of the cement and fly ash are reported in table 1. Helium pycnometry was used to determine the densities and Brunauer-Emmett-Teller (BET) surface area measurements were obtained using nitrogen (2 % coefficient of variation for 3 replicate samples (Gurney et al., 2012)). Particle size was determined by laser diffraction in isopropanol and characterized by the D_{10}, D_{50} (median), D_{90} percentile diameters. The fine limestone powder has a median particle size of 1.6 µm and a reported density of 2700 kg/m^3. The BET surface area is 9.93 m^2/g. The limestone is a high purity natural calcium carbonate with 98 % by mass $CaCO_3$. The concrete mixtures are designed assuming 2 % (entrapped) air content and targeting a 28 d compressive strength of 40 MPa and a 150 mm nominal slump. The details of the mixture proportions are given in table 2. The ratio of fine to coarse aggregate is constant for all the concrete mixtures. To minimize the volume of cement used in the concrete, the aggregate content of the three OPC mixtures was varied from 70 % to 75 % in 2.5 % increments. This produced a 10.4 % and 17.1 % reduction in cement volume over the initial, 70 % aggregate concrete. The concrete mixture with 75 % aggregate experienced substantial bleeding and segregation, due to the low paste volume and large dosage of high range water reducing admixture (HRWRA) required to achieve the target slump. This mixture represents the upper limit of aggregate content and is not deemed feasible in a construction scenario without the use of stabilizers.

The addition of fly ash and limestone into the concrete increases the cohesiveness of the mix. As such, the aggregate content of the HVFA concrete was maintained near 75 % to reduce the required volume of the cement. The class F fly ash concrete reduced the

cement volume by 44.5 % and the class C fly ash concrete reduced the cement volume by 45.2 %, relative to the 70 % aggregate OPC concrete. To achieve the desired 1 d strengths, the *w*/*cm* of the HVFA concrete mixtures was reduced relative to the control concrete. The water reduction is greater for the class F fly ash as it is less reactive than the class C fly ash. For the HVFA concretes, a 40 % volumetric replacement of cement by fly ash/limestone is utilized where a 3:1 volumetric ratio of fly ash to limestone is maintained. Compressive strengths of the concrete mixtures are given in table 3. Compression test are conducted in compliance with ASTM C39. Further analysis of the concrete mixtures, including the use of a Type III cement to increase early-age strengths, can be found elsewhere (Bentz et al., 2015).

Table 1: Characteristics of the cement and fly ash.

% mass	Type I	Class F Fly ash	Class C Fly ash
CaO	64.2	0.7	24.6
SiO_2	20.86	59.7	38.4
Al_2O_3	4.77	30.2	18.7
Fe_2O_3	2.05	2.8	5.1
MgO	3.09	0.8	5.1
SO_3	2.81	0.02	1.4
LOI	1.13	0.8	0.3
Total alkalies	0.46	1.78	2.09
Blane Fineness (m^2/kg)	401	Not Reported	
D_{10},D_{50}, D_{90} (μm)	1.4,13.0,42.3	1.7,18.4,83.1	0.9,8.6,50.2
Density (kg/m^3)	3150±10	2490±10	2650±10
BET Surface Area (m^2/g)	1.14	1.28	0.9

Table 2: Mixture proportions for concrete (kg/m^3 or L/m^3 for HRWRA). For computing *w*/*cm*, cementitious materials include cement, fly ash, and limestone.

Mixture	Cement	Cement Reduction	Fly ash	Limestone	Water	w/cm	Fine Agg.	Coarse Agg.	Glenium 7710[1]	Viscocrete[1]
Control - 70 % Agg	396.5	-	-	-	158.6	0.40	850	1029	2.08	-
Control - 72.5 % Agg	355.1	10.4 %	-	-	142.0	0.40	886	1073	2.20	0.35
Control - 75 % Agg	328.7	17.1 %	-	-	131.5	0.40	909	1101	1.90	0.92
Class F Fly Ash/Limestone	220.0	44.5 %	86.9	31.4	114.0	0.34	915	1107	1.37	1.46
Class C Fly Ash/Limestone	217.2	45.2 %	91.3	31.0	125.6	0.37	904	1094	1.35	0.90

2.2. Concrete Diffusivity Measurements

Estimating the diffusivity of the concrete can be achieved through measurements of both the bulk concrete resistivity and the pore solution resistivity. The resistivity of the concrete mixes is measured by placing a sample of the fresh concrete into a 10 cm diameter by 20 cm long standard plastic cylinder mold. Two parallel stainless steel rods are inserted through the lid of the mold and into the fresh concrete. The resistance is measured with a Giatec Scientific RCON[1] resistivity meter at intervals of 5 min for the first 24 h at 10 kHz. The resistivity cell is calibrated using KCl solutions with known resistivity.

Measurements of pore solution resistivity are made by extracting pore solution from hydrated paste with the same cement, fly ash, and limestone proportions as the

[1] Certain commercial products are identified in this paper to specify the materials used and the procedures employed. In no case does such identification imply endorsement or recommendation by the National Institute of Standards and Technology, nor does it indicate that the products are necessarily the best available for the purpose.

concrete mixtures (Barneyback and Diamond, 1981). Cylinders of paste 4 cm in diameter and 7 cm long were cast and sealed in plastic containers and stored at 23 ^oC. To extract the pore solution, the cylinders are removed from their container and placed into a large steel cylinder die. The cylinder die is bolted on top of a hardened steel plate, with grooves to allow fluid movement, and the assembly is placed into a universal testing machine. A steel ram is placed on top of the paste cylinder and the load is gradually increased. As the load increases, pore solution is expelled from the paste cylinder. Nitrogen pumped through the assembly moves the pore solution through the grooves in the bottom plate and into a collection container.

Table 3: Average compressive strength (standard deviation) of three 10 *cm* diameter by 20 *cm* long cylinders. Compressive strengths are given in units of *MPa*.

Mixture	1 d	7 d	28 d	90 d
Control - 70 % Agg.	22.1 (3.0)	not meas.	42.9 (1.4)	54.8 (5.8)[2]
Control - 72.5 % Agg.	22.2 (1.0)	30.4 (7.0)	41.8 (2.4)[2]	52.6 (13.1)
Control - 75 % Agg.	18.9 (0.4)	26.9 (8.8)	26.3 (3.6)	23.2 (6.3)
Class F Fly Ash/Limestone	23.0 (1.8)[2]	28.5 (1.8)	38.9 (10.8)[2]	56.0 (9.5)
Class C Fly Ash/Limestone	18.7 (3.0)[2]	27.0 (1.7)[2]	43.9 (2.6)	44.1 (3.7)

[2]Average of two as opposed to three replicate specimens.

Approximately 1 mL to 2 mL of pore solution is extracted per sample. The extracted solution is filtered through a 0.2 μm inorganic membrane filter to remove fine cement particles. The resistivity cell consists of a plastic tube with two parallel 560 μm platinum wires inserted transversely through the tube and spaced at a distance of 3 cm. The cell is calibrated with standard solutions of KCl with known resistivity. The complex impedance of the pore solution is measured using a sinusoidal voltage with an amplitude of 0.5 V and frequency ranging from 1 kHz to 3 MHz. The bulk resistance of the sample is determined from the real component of the impedance, as the frequency where the imaginary component of the impedance is closest to the abscissa. The diffusivity is computed by the Nernst-Einstein equation, equation 1, where ρ_c is the bulk concrete resistivity, ρ_o is the pore solution resistivity, D_0 is the self-diffusivity of chloride ions in water, and D_c is the bulk concrete diffusivity.

$$\rho_c / \rho_o = D_o / D_c \quad (1)$$

For the simulations that follow, $D_0 = 1.89 \times 10^{-9}$ m^2/s at 23 ^oC (Mills, 1989) and D_c is computed from the experimental measurements of resistivity.

2.3. Chloride Binding

Chloride binding was measured by sieving the fresh concrete through a # 8 sieve. The obtained mortar was cast into 25 mm cubes and cured for 28 d in a sealed container. At 28 d, the cubes were ground to a fine powder and dried for 4 d at 40 ^oC and 9 % relative humidity. After the drying, approximately 30 g of the ground mortar was placed into 250 mL of sodium chloride solutions with nominal molar concentrations of 0.01 mol/L, 0.05 mol/L, 0.10 mol/L, 0.25 mol/L, 0.50 mol/L, 0.75 mol/L, 1.00 mol/L, and 1.50 mol/L. At 90 d past the mixing date, 5 mL of each sodium chloride solution was removed and diluted with 5 mL of de-ionized water. A chloride ion selective probe was used to measure the chloride

concentration. The difference between the nominal storage solution concentration and the concentration at 90 d represents the amount of chlorides bound to the cement paste.

2.4. Neutron Tomography

To study the penetration of methacrylate and epoxy crack fillers, 5 cm x 5 cm x 15 cm OPC mortar beams, with w/c = 0.4 and reinforced with a stainless steel threaded rod, were cast and cured in sealed conditions. A single crack was created by loading the beam in 3-point bending. The size of the crack is controlled by limiting the maximum load applied to the beam. The average crack mouth opening, measured after removing the load using optical microscopy, was measured to be 351 μm (standard deviation 25 μm on 10 measurements) for the epoxy-filled crack and 242 μm (standard deviation 16 μm on 10 measurements) for the methacrylate-filled crack. The cracks were filled by ponding approximately 5 mL of the crack filler on the crack opening. After 14 d, a 6 mm diameter coring bit was used to core the crack. Neutron tomography measurements were made at the NIST neutron imaging facility (Jacobson et al., 2008). The core is placed into a neutron beam with a fluence rate of 1.37 x 10^7 $cm^{-2}s^{-1}$ and collimation ratio of 450. A gadolinium oxysulfide scintillator converts the neutrons to light that is captured by a complimentary metal oxide semiconductor camera. The lens used to focus the light to the camera produces an effective pixel pitch of 15 μm. The specimen is rotated 180° in 0.25° increments with five images (20 s exposure) taken at each point. The five images are averaged and three-dimensional tomographic reconstruction is performed using the filtered back projection algorithm.

3. Simulation Procedure

3.1. Description of Mathematical Model

The concrete considered in this model is assumed to be at a constant degree of saturation, and the transport of chloride ions dominated by diffusion; transport due to advection resulting from capillary suction or interactions between ions present in the pore solution are not incorporated into the model. Derivation of the model begins with a mass balance on an infinitesimal control volume of the concrete domain. Figure 1 shows schematic representations of the domain representing the cracked concrete and the control volume. In figure 1b, the flux across a face of the control volume is $\boldsymbol{j_i}$. The time rate of change of the chloride concentration in the control volume is equal to the flux going into the control volume, minus the flux going out, plus accumulation of the chloride inside the control volume. Equation 2 expresses this statement in terms of the free chloride concentration. Fick's Law, combined with the continuity equation, give the rate change in the chloride concentration.

$$\frac{\partial C_f}{\partial t} = \nabla \cdot \left(D_{con}(t) \nabla C_f\right) + k\left(C_{bound-eqbm} - C_{bound}\right) \quad (2)$$

In equation 2, the sink resulting from chloride binding is modeled by a first order reaction with the difference between the equilibrium bound chlorides $\left(C_{bound-eqbm}\right)$ and the chlorides previously bound $\left(C_{bound}\right)$. The change in concentration of bound chlorides is described in equation 3, where k is the reaction rate constant.

$$\frac{dC_{bound-eqbm}}{dt} = k\left(C_{bound} - C_{bound-eqbm}\right) \quad (3)$$

The relationship between the free chloride concentration and the concentration of chlorides that react with the cement paste is modeled with a Langmuir isotherm, equation 4, with α and β determined by fitting equation 4 to experimental data.

$$C_{bound} = \frac{\alpha C_f}{1 + \beta C_f} \tag{4}$$

At each time step, equations 2 and 3 are solved simultaneously. The total chloride concentration at a given time step is the sum of the bound and free chlorides $\left(C_{total} = C_f + C_{bound-eqbm}\right)$. Equation 2, with $k = 0$ signifying that no binding is occurring inside the crack, describes the chloride concentration inside the crack. When the crack is saturated, the diffusivity of the crack is set to $2D_0$ to account for advection of chloride ions due to water movement. When the crack is filled with methacrylate or epoxy, the diffusivity of the crack is set to the diffusivity of chloride ions in the corresponding crack-filling polymer.

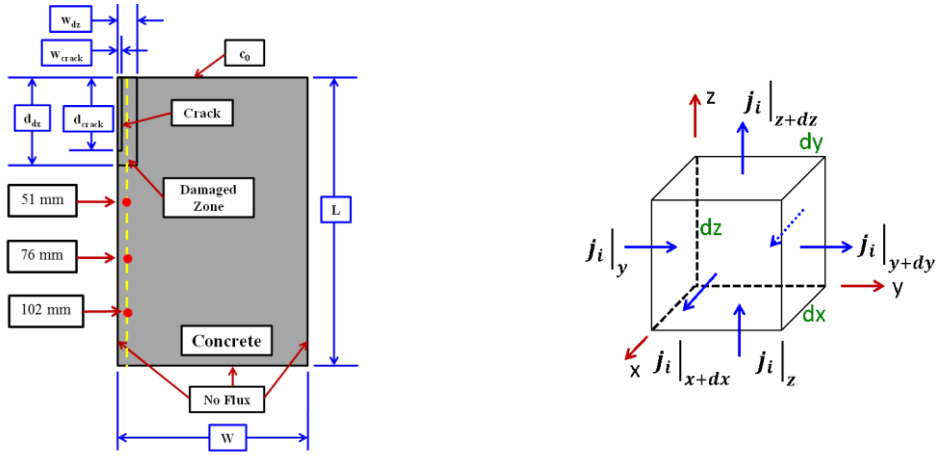

(a) Model Domain (b) Control Volume

Figure 1: Schematic diagrams of the (a) domain representing the crack concrete system and (b) the infinitesimal control volume used to derive the governing equations.

The chloride ion diffusivity of the methacrylate and the epoxy is estimated from the diffusivity of water in these polymers by assuming the ratio of the crack filler's water diffusivity to chloride ion diffusivity is equal to the ratio of water's self-diffusivity to chloride ion diffusivity in water. The water diffusivities for methacrylate and epoxy were taken from (Parthasarathy et al., 2012) and (Coniglio et al., 2013), and the water self-diffusivity and chloride diffusivity values were taken from (Holz et al., 2000) and (Woolf, 1963). The model assumes a damaged zone (DZ) immediately surrounds the crack and has a chloride diffusivity 20 times the bulk concrete diffusivity$\left(D_{DZ} = 20D_{con}(t)\right)$. The larger bulk diffusivity in this damaged zone is to account for the presence of micro-cracking and exposed pores resulting from the formation of the crack. A detailed study of the effect of the damaged zone on service life predictions resulting from this type of model is given in (Jones et al., 2015). Experimental evidence for the existence of a damaged zone is given elsewhere (Bentz et al., 2013; Şahmaran and Özgür, 2008). The size of the damage zone has been calibrated to match experimental results from the studies in (Şahmaran and Özgür,

2008). In the present study, both the diffusivity and chloride loading are assumed to be functions of time. To improve the convergence of the numerical simulations, equation 5 is fit to the measured diffusivity.

$$D_{con}(t) = \begin{cases} D_s & t \leq 3.5\ h \\ D_\infty + D_i t^{-m} & t > 3.5\ h \end{cases} \quad (5)$$

In equation 5, D_s is the diffusivity at the early age, $t \leq 3.5\ h$, and is assumed to be constant. D_∞, D_i, and m are parameters fit to the diffusivity measurements. The chloride loading at the top boundary is assumed to be a sinusoidal function, equation 6, where $C_{top}(t)$ is the chloride concentration at the top boundary and *t* is the time in months.

$$C_{top}(t) = 3380 + 1070 \cos\left(\frac{\pi t}{6}\right)\ mol/m^3 \quad (6)$$

Equation 6 was determined from measurements of Utah bridges decks in (Guthrie et al., 2011). The boundary conditions at the left, right, and bottom surfaces are set such that the mass flux is zero, so that chloride movement is from the top surface to the bottom.

3.2 Simulation Approach

This study seeks to assess the effectiveness of methacrylate and epoxy concrete crack fillers on the service life of reinforced concrete structures. Several model parameters are varied to study their effect on the chloride distribution around the crack. Two model scenarios served as a basis of comparison for models simulating HVFA concretes and concretes with cracks. The base-case configuration does not contain a crack as it studied the effects of the concrete mixture proportions. The saturated crack configuration is the reference for the methacrylate and epoxy filled crack simulations which also looked at the effect of the concrete mixture proportions. This base-case configuration was run for each concrete to show the effect of the reduced diffusivity seen in the HVFA concrete. The interaction between the crack filler and the surrounding concrete is investigated in this study. Based on neutron tomography data, the DZ diffusivity is set equal to the concrete diffusivity when the crack filler is present in the crack. This implies that the crack filler fills and seals open porosity created when the flexure crack is formed. The parameters studied in this work are given in table 4.

4. Results and Discussion

4.1. Diffusivity

The concrete diffusivity is estimated from equation 1 and its time-dependence is determined from fitting the pore solution resistivity measurements (figure 2a) to a function of the form $y = A \cdot t^b$ for $t > 3.5\ h$. A non-linear regression of the diffusivity values and equation 5 produced the parameters in Table 5. The quality of the regression is determined by computing the standard error of the residuals, the difference between the fitted curve and the measured values. The standard errors of the residuals are small, compared to the estimated values, which implies that the assumed functional form of the time-dependent diffusivity is suitable for use in the numerical simulations. The pore solution resistivities and concrete diffusivities are plotted, in figure 2, along with the chloride-binding isotherm. For the OPC concretes, the paste composition is the same - only the volume fraction of the aggregates is varied. Because of this, the pore solution composition is assumed to be the same among the control concrete mixtures. The

differences among diffusivity values for the control mixtures are within a factor of 2. Pore solution resistivity data are shown in figure 2a. OPC concrete has a lower resistivity than the fly ash concretes. This is because the fly ashes contain fewer soluble (alkali) ions than the cement.

Table 4: Parameters used in service life model.

Variable	Value	Description
$D_{con}(t)$	equation 5	Diffusivity as a function of time for each concrete mixture
D_{crack}	$4.0 \cdot 10^{-9}\ m^2/s$	Saturated with Cl^- solution
	$2.0 \cdot 10^{-12}\ m^2/s$	Methacrylate filled crack
	$1.0 \cdot 10^{-13}\ m^2/s$	Epoxy filled crack
d_{crack}	40.0 mm	Crack depth
w_{crack}	250.0 μm	Width of crack with depth 40 mm
d_{damage}	44.0 mm	Depth of DZ with crack depth 40 mm
w_{damage}	4.25 mm	Width of DZ with crack depth 40 mm
$C_{top}(t)$	equation 6	Cl^- concentration at top surface
α, β	table 6	Langmuir Parameters, equation 4
L	204.0 mm	Concrete thickness
W	100.0 mm	Width of section
k	$1 \cdot 10^{-7}\ 1/s$	Cl^- binding reaction rate constant

Table 5: Diffusivity parameters determined from nonlinear regress to fit data to model.

	D_s	D_∞	D_i	m	Residual STD. Error
Control – 70.0 % Agg	$1.39 \cdot 10^{-10}$	$2.12 \cdot 10^{-12}$	$1.96 \cdot 10^{-10}$	-0.88	$4.40 \cdot 10^{-13}$
Control – 72.5 % Agg	$1.31 \cdot 10^{-10}$	$2.19 \cdot 10^{-12}$	$2.03 \cdot 10^{-10}$	-0.90	$4.18 \cdot 10^{-13}$
Control – 75.0 % Agg	$1.14 \cdot 10^{-10}$	$1.79 \cdot 10^{-12}$	$1.48 \cdot 10^{-10}$	-0.75	$4.83 \cdot 10^{-13}$
Class F Ash/Limestone	$9.45 \cdot 10^{-11}$	$9.45 \cdot 10^{-13}$	$1.83 \cdot 10^{-10}$	-0.71	$7.77 \cdot 10^{-13}$
Class C Ash/Limestone	$8.37 \cdot 10^{-11}$	$5.64 \cdot 10^{-13}$	$2.52 \cdot 10^{-10}$	-0.77	$6.92 \cdot 10^{-13}$

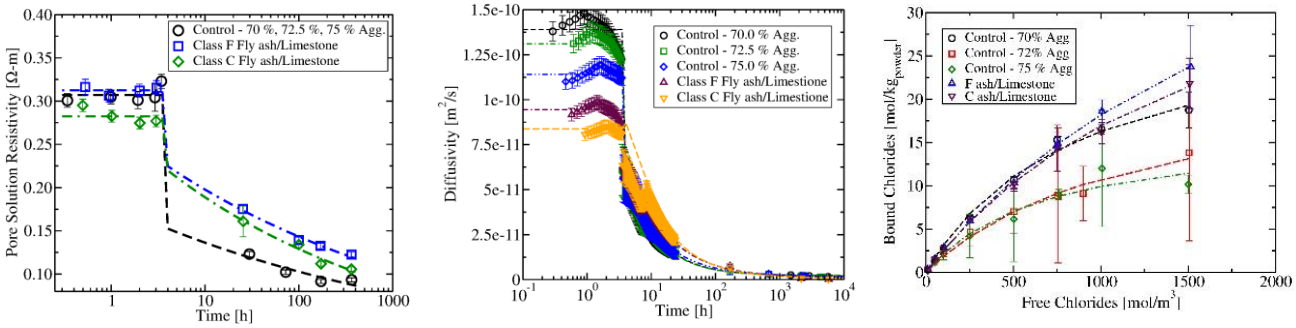

(a) Pore Soln. Resistivity (b) Concrete Diffusivity (c) Chloride Binding

Figure 2: Pore solution resistivity, concrete diffusivity, and chloride binding measurements. (a) Measured pore solution resistivity. (b) Diffusivity of concrete mixtures. (c) Chloride binding isotherm expressed in mol/kg of powder: cement, fly ash, and limestone. Error bars are the measurement uncertainty for replicates.

At early ages ($t \leq 3.5\ h$) the diffusivity of the HVFA concretes are less than the OPC concretes. Between $t = 3.5\ h$ and $t = 30\ h$, the diffusivities of all concretes are approximately equal. For $t > 30\ h$, the diffusivity of the HVFA mixtures becomes lower than the control OPC mixtures. The D_∞ parameters in table 5 are a factor of 2 to 4 times

smaller for the fly ash concrete mixtures. The lower the D_∞, the longer it takes for chloride ions to move through the concrete matrix, which has a positive effect on the service life.

4.2 Chloride Binding

The amounts of chloride ions bound to the cement paste as a function of concentration are given in figure 2c. The control mixture with 70 % aggregates and HVFA mixtures are capable of binding more chlorides than the two control mixtures with 72.5 % and 75 % aggregates. This may be a result of the higher dosage of HRWRA used in these latter two mixtures. This result requires further research as it will play an important role in the predicted service life. The measurement uncertainty is large for some data points, but there is an observable difference between the control concrete with 72.5 % and 75 % aggregates and the HVFA concretes. The chloride binding is assumed to follow a Langmuir isotherm with parameters given in table 6, determined by non-linear regression.

Table 6: Langmuir isotherm parameters determined by non-linear regression analysis.

Mixture	α	β	Residual STD. Error
Control – 70.0 % Agg	$3.49 \cdot 10^{-2}$	$1.14 \cdot 10^{-3}$	0.6248
Control – 72.5 % Agg	$2.99 \cdot 10^{-2}$	$0.85 \cdot 10^{-3}$	0.6451
Control – 75.0 % Agg	$2.46 \cdot 10^{-2}$	$1.49 \cdot 10^{-3}$	1.081
Class F Ash/Limestone	$2.61 \cdot 10^{-2}$	$0.44 \cdot 10^{-3}$	0.3045
Class C Ash/Limestone	$2.67 \cdot 10^{-2}$	$0.58 \cdot 10^{-3}$	0.4114

4.3 Chloride Threshold

For this study, the service life is defined to be the time required for the Cl^- concentration to reach a certain proportion of the OH^- ion concentration in the pore solution immediately surrounding the steel reinforcement. Hydroxyl ion concentration is measured by assessing the pH of the pore solution and converting to OH^- concentration by the Sørensen definition of pH, which is based on concentration rather than the ion activity. The OH^- concentration in the pore solution was measured at 5 time points ranging from 24 h to 700 h. By 400 h, the OH^- concentration begins to plateau. For service life calculations, the OH^- is determined by taking the average of the last two measurements for each paste mixture and is reported in table 7. The values obtained in table 7 are in good agreement with the trends reported elsewhere (Diamond, 1981; Shehata et al., 1999) and the measured OH^- concentrations are within the same order of magnitude of one another. The chloride threshold values used in this study are given in table 7. Three service life scenarios are considered; the case where a black rebar is embedded into concrete; the use of a calcium nitrite ($Ca(NO_2)_2$) corrosion inhibitor; and the use of epoxy coated rebar. Each scenario has an associated chloride concentration at which corrosion will begin (C_{crit})typically expressed as a ratio to the OH^- concentration. For the case of the black steel rebar, the critical threshold level is assumed to be $[Cl^-]/[OH^-] = 0.6$ (Hausmann, 1976). This assumption is made for the OPC mixtures as well as the HVFA mixtures. There is some disagreement in the literature regarding the critical threshold level as some report lower C_{crit} values (Oh et al., 2003; Thomas, 1996) and others report similar or larger values for C_{crit} (Alonso et al., 2002; Schiessl and Breit, 1996). Service lives of concretes with calcium nitrate are calculated based on 3 % dosage, by mass of cementitious material.

When corrosion inhibitors are used, the critical chloride threshold occurs when the concentration of chloride ions is equal to the concentration of nitrate ions (Ann and Song, 2007; Gonzalez et al., 1998). For the case of an epoxy coated rebar, the chloride threshold level reported in (Al-Amoudi et al., 2004) corresponds to the initiation of corrosion of a bar with 1 % damage to its coating and is reported to be 2 % Cl^- per mass of cement. This study assumed the chloride threshold to be 2 % per mass of powder and converted to mol/m^3 in table 7.

Table 7: The concentration of chlorides at which corrosion is assumed to begin.

Mixture	$[OH^-]$ mol/m^3	Cl^- Threshold	C_{crit} mol/m^3	$[Cl^-]/[OH^-]$
Control – 70 %, 72.5 %, 75 % Agg.	1087	Black Rebar	652	0.6
		Corrosion Inhibitor	1136	1.1
		Epoxy-coated Rebar	1411	1.3
Class F Ash/Limestone	733	Black Rebar	440	0.6
		Corrosion Inhibitor	1296	1.8
		Epoxy-coated Rebar	1576	2.2
Class C Ash/Limestone	958	Black Rebar	575	0.6
		Corrosion Inhibitor	1228	1.3
		Epoxy-coated Rebar	1525	1.6

4.4 Neutron Tomography

Figure 3a is the neutron tomography image of an extracted core sample. In Figure 3a, the methacrylate appears as a lighter color running vertically down the center of the sample. From this image, it appears that methacrylate is able to penetrate the full length of the crack and there appears to be good contact between the surface of the crack and the crack filler; no voids are visible at the interface. To view the interior of the crack, the mortar is removed from the image by only displaying voxels with attenuation values above a certain threshold. Because the crack filler has a stronger neutron attenuation than the mortar, its voxels are easily distinguished from the surrounding substrate.

(a) Full Specimen (b) Methacrylate

Figure 3: Neutron tomography of methacrylate filled crack. (a) extracted core and (b) mortar removed to show methacrylate (two views of the same crack).

Figure 3b shows the crack filler with the mortar substrate removed from the image. The textured and rough surface of the methacrylate indicates that the crack filler is in good

contact with the crack face. The crack filler seals and fills the observable surface irregularities. The extent of the crack filler penetration into the mortar is not apparent from these images, but it does support the assumption that the crack filler can restore the DZ diffusivity to its original value by sealing open porosity generated during crack formation. Figure 3b also reveals several voids in the interior of the crack filler. The model assumes that the crack filler is homogeneous and defect free. Figure 3b suggest that this assumption is not fully correct. The figure also shows that as the crack filler reaches the bottom of the crack, the methacrylate becomes less homogeneous, suggesting there is a minimum crack size that the crack filler can penetrate effectively.

Figure 4 shows the neutron tomography images of an epoxy filled crack. The epoxy penetrates the crack and makes good contact with the crack surface with no voids visible in figure 4a. The surface of the epoxy is textured, suggesting that the crack filler seals and fills the surface topography of the crack face. Figure 4b shows two large defects in the crack, both of which are around large voids in the mortar. The image shows that the crack filler wicked around the surface of the voids to continue filling the crack. The interior of the crack filler is continuous, defect free, and fills the full length of the crack. The viscosity of the epoxy is approximately 10 times the viscosity of the methacrylate. This suggests that the ability of the crack filler to fill the crack is dependent on both the crack size (both length of the crack and crack mouth opening) and crack filler viscosity.

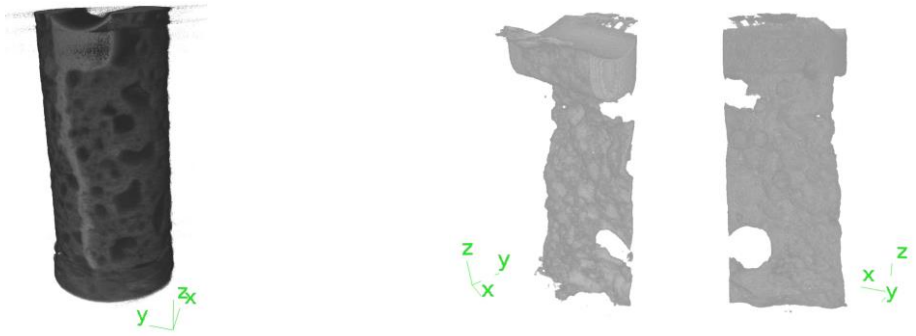

(a) Full Specimen (b) Epoxy

Figure 4: Neutron tomography of epoxy filled crack. (a) extracted core and (b) mortar removed to show epoxy (two views of the same crack).

4.5. Chloride Ingress and Service Life Calculations – Base Case

Figure 5 shows the calculated free chloride concentration at a cover depth of 51 mm for each concrete mixture. These simulation results are for the case of an un-cracked concrete and serve as the basis for comparison to the cracked concrete cases. In figure 5, the chloride concentration in the OPC concretes is higher than that in the HVFA concretes at any given time point. This is to be expected because D_∞ for the OPC concrete is larger than D_∞ for the HVFA concrete. The OPC control concrete containing 75 % aggregate had a D_∞ less than the 70 % aggregate and 72 % aggregate, resulting from the increased tortuosity of the pore structure due to the additional aggregate content. By contrast, the binding capacity of the 75 % aggregate OPC control is lower than the other two control concrete mixtures because of the lower paste content, which means that more chloride ions remain in the pore solution. The OPC control concrete with 75 % aggregate had the lowest

service life of the OPC concretes. This suggests that chloride binding cannot be neglected, as its effect on chloride concentration can be greater than the effect of a lower diffusivity.

Table 8 shows the estimated service life of each concrete mixture. The addition of the fly ash to the concrete decreases the diffusivity and increase the binding capacity of the paste. This resulted in a lower free chloride concentration at a given depth and time which results in a longer service life. The class F fly ash concrete has an OH^- concentration 33 % lower than the OPC concretes and requires a lower chloride ion concentration to initiate corrosion. The service lives in table 8 and free chloride concentration in figure 5 suggest that the decreased diffusivity and increased binding capacity are the dominant factors that determine service life.

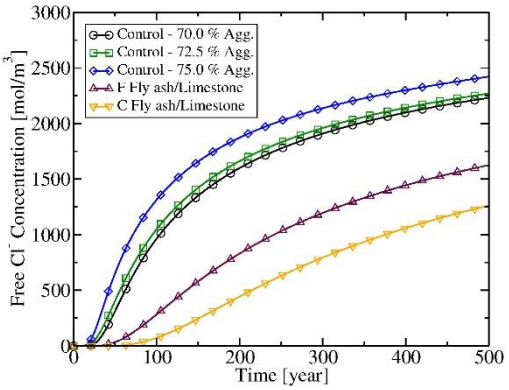

Figure 5: Free chloride concentration at a cover depth of 51 *mm* in un-cracked concrete.

The class C fly ash concrete has similar binding characteristics to the class F concrete, but its diffusivity is lower and OH^- concentration is higher. This results in a service life at 51 *mm* cover and with black rebar that is 46 % higher than the class F fly ash concrete and 69 % higher than the OPC concrete with 70 % aggregate. Selecting the appropriate fly ash and cement to produce a concrete with a high OH^-concentration and low diffusivity is important for the durability of the concrete structure. Concretes containing at least 40 % of the volume of cement replaced with fly ash reduce the rate of chloride ingress and increase the time to reach the critical chloride threshold level.

4.6. Chloride Ingress and Service Life Calculations – Cracked Case

Figure 6 shows the simulated free chloride concentration in the control concrete with 70 % aggregate volume fraction. As shown in Figure 6a, the presence of a crack in the concrete cover plays a significant role in chloride diffusion through the concrete. The crack acts as a conduit for chloride ions to bypass a portion of the concrete and travel quickly to the bottom of the crack. The presence of the DZ around the crack allows chloride ions to traverse farther into the concrete though the crack opening faces faster than through the concrete - represented mathematically by setting $D_{DZ} = 20D_{con}$. This has the effect of increasing the effective crack size beyond its assumed 500 µm opening. Filling the crack with a methacrylate or epoxy crack filler can reduce the chloride concentration to levels approximately equal to the base case levels. This is because the diffusivities of both the methacrylate and epoxy are approximately equal to the D_∞ term in equation 5 (Jones et al.,

2015). Previous simulation studies have focused on the influence of the DZ diffusivity on the predicted service life and suggested that the DZ play a significant role (Jones et al., 2015). Based on the neutron tomography results, which suggest that the crack filler can uniformly coat the crack surfaces, the model assumes that the DZ diffusivity is restored to the concrete diffusivity. This implies that the crack filler blocks chlorides from entering the concrete through the crack faces via open porosity and micro cracking. Taking this assumption, the free chloride concentrations in Figures 6b and 6c are shown for the methacrylate and epoxy crack filler, respectively.

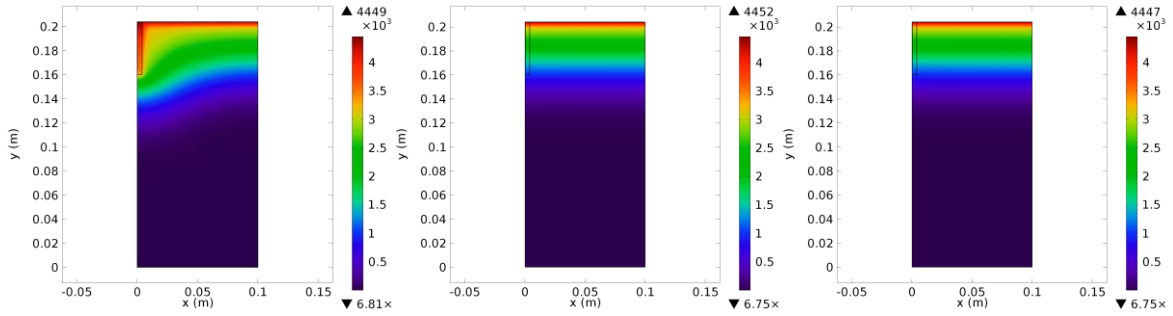

(a) Saturated Crack (b) Methacrylate (c) Epoxy

Figure 6: Free chloride concentration in 70 % aggregate control concrete mixture at 75 years for the case of (a) a crack saturated with chloride solution, (b) a crack filled with a methacrylate crack filler, and (c) a crack filled with an epoxy crack filler. The presence of a crack in the cover significantly increases the chloride ion concentration near the 51 *mm* cover depth.

Table 8: Service life (years) of concrete without a crack (base case) and with a crack in cover for all concrete mixtures and with methacrylate and epoxy crack fillers.

Mixture	Cl^- Threshold	Base Case			Saturated Crack			Methacrylate			Epoxy		
		51 *mm*	76 *mm*	102	51 *mm*	76 *mm*	102	51 *mm*	76 *mm*	102	51 *mm*	76 *mm*	102
Control 70 % Agg	Black Rebar	73	163	293	4	72	195	73	162	293	73	163	294
	Corrosion	127	282	> 500	9	143	352	127	282	> 500	128	283	> 500
	Epoxy-coated	161	358	> 500	14	187	446	161	375	> 500	162	358	> 500
Control 72.5 % Agg	Black Rebar	66	147	266	6	65	218	66	147	265	66	148	266
	Corrosion Inhibitor	117	260	467	9	131	363	117	259	466	117	260	467
	Epoxy-coated	148	330	> 500	13	172	453	148	330	> 500	149	331	> 500
Control 75.0 % Agg	Black Rebar	50	112	203	3	49	134	50	112	203	50	112	203
	Corrosion Inhibitor	88	196	354	6	98	244	88	196	354	88	197	354
	Epoxy-coated	112	249	443	9	129	310	11	249	442	112	250	443
Class F Ash/Limestone	Black Rebar	126	283	> 500	4	106	320	124	282	> 500	126	284	> 500
	Corrosion Inhibitor	345	> 500	> 500	20	381	> 500	342	> 500	> 500	347	> 500	> 500
	Epoxy-coated	492	> 500	> 500	36	> 500	> 500	487	> 500	> 500	494	> 500	> 500
Class C Ash/Limestone	Black Rebar	234	> 500	> 500	7	208	> 500	230	> 500	> 500	236	> 500	> 500
	Corrosion Inhibitor	491	> 500	> 500	24	> 500	> 500	483	> 500	> 500	493	> 500	> 500
	Epoxy-coated	> 500	> 500	> 500	42	> 500	> 500	> 500	> 500	> 500	> 500	> 500	> 500

Table 8 shows the calculated service life for each concrete mixture at cover depths of 51 mm, 76 mm, and 102 mm. For each concrete mixture, the saturated crack reduces the service life to approximately 4 years at a cover depth of 51 mm. Because the diffusivity of the crack is several orders of magnitude larger than the concrete, the crack negates any

advantage seen from using high-performance, low diffusivity concrete mixtures. This effect is observed for all cover depths and emphasizes the importance of repairing cracks before they can become large enough to affect the service life. Filling the crack with the crack filler does restore the service life. The diffusivity of the methacrylate crack filler is larger than the diffusivity of the epoxy. With concretes that have a low diffusivity, the methacrylate cannot fully restore the service life. This suggests that that the most effective repair occurs when the diffusivities of the crack filler and the concrete are approximately equal. Using a crack filler with a larger diffusivity does not restore the effectiveness of the cover because the crack filler becomes the preferred chloride ingress route.

5. Conclusion

Simulation results suggest HVFA concretes can have a service life greater than their OPC counterparts. This is a result of a decreased diffusivity and an increased chloride binding, both of which are responsible for decreasing the free chloride ion concentration at a given depth and time. Increasing the aggregate volume fraction of the concrete acts to decrease its diffusivity, however, these concretes had a measurably lower chloride binding capacity. This may be a result of the increased use of HRWRA to maintain the target slump. As a result, the free chloride ion concentration is greater than the concretes that used less HRWRA at a given depth. This suggests that the use of HRWRA can affect service life and must be accounted for in service life models.

A crack in the concrete cover will reduce the service life of the structure by providing a preferential pathway for chloride ions to reach the reinforcement. Filling the crack with an epoxy or methacrylate material can restore the service life capacity of the concrete. Neutron tomography results suggest the crack filling material fills the porosity exposed by the formation of the crack. This behavior is represented in the simulation by restoring the DZ diffusivity to the bulk concrete diffusivity. Methacrylate crack fillers are able to penetrate and fill the crack volume, but voids are present in the crack filler and increase in frequency as the crack narrows. Epoxy crack fillers filled the volume of the crack without void formation. The appropriate choice of crack filler is dependent on the relative diffusivity of the crack filler to bulk concrete and size and length of the crack. Further research is required to understand the relationship between crack filler properties and their ability to fill and seal cracks.

References

Omar Saeed Baghabra Al-Amoudi, Mohammed Maslehuddin, , and Mohammad Ibrahim. Long-term performance of fusion-bonded epoxy-coated steel bars in chloride-contaminated concrete. *ACI Materials Journal*, 101:303–309, 2004. doi: 10.14359/13364.

C. Alonso, M. Castellote, and C. Andrade. Chloride threshold dependence of pitting potential of reinforcements. *Electrochimica Acta*, 47:3469–3481, 2002.

Ki Young Ann and Ha-Won Song. Chloride threshold level for corrosion of steel in concrete. *Corrosion Science*, 49:4113–4133, 2007.

R.S. Barneyback and Sidney Diamond. Expression and analysis of pore fluids from hardened cement paste and mortars. *Cement and Concrete Research*, 11:279–285, 1981.

Dale P. Bentz, Chiara F. Ferraris, and Kenneth A. Snyder. Best practices guide for high-volume fly ash concretes: Assuring properties and performance. Technical report, National Institute of Standards and Technology, 2013. NIST Technical Note **1812**.

Dale P. Bentz, Edward J. Garboczi, Yang Lu, Nicos Martys, Aaron R. Sakulich, and W. Jason Weiss. Modeling of the influence of transverse cracking on chloride penetration into concrete. *Cement and Concrete Composites*, 2013.

Dale P. Bentz, Scott Z. Jones, and Kenneth A. Snyder. Design and performance of ternary blend high-volume fly ash concretes of moderate slump. *Submitted to Construction and Buliding Materials*, 2015.

N. Coniglio, K. Nguyen, R. Kurji, and E. Gamboa. Characterizing water sorption in 100 % solids epoxy coatings. *Process in Organic Coatings*, 76:1168–1177, 2013.

Mustafa Şahmaran and Yaman Özgür. Influence of transverse crack width on reinforcement corrosion initiation and propagation in mortar beams. *Canadian Journal of Civil Engineering*, 35(3):236–245, 2008.

D. Darwin, J. Browning, and W.D. Lindquist. Control of cracking in bridge decks observations from the field. *Cement and Concrete Aggregate*, 2:148–154, 2004.

Sidney Diamond. Effects of two Danish flyashes on alkali contents of pore solutions of cement- flyash paste. *Cement and Concrete Research*, 11:383–394, 1981.

J.A. Gonzalez, E. Ramirez, and A. Bautista. Protection of steel embedded in chloride containing concrete by means of corrosion inhibitors. *Cement and Concrete Research*, 28:577–589, 1998.

Lisa R. Gurney, Dale P. Bentz, Taijiro Sato, and W. Jason Weiss. Reducing set retardation in high volume fly ash mixtures with the use of limestone: Improving constructability for sustainability. *Transportation Research Record, Journal of the Transportation Board*, No. 2290:139–146, 2012.

W. Spencer Guthrie, Curtis D. Nolan, and Dale P. Bentz. Effect of initial scarification and overlay treatment timing on chloride concentration in concrete bridge decks. *Transportation Research Record: Journal of the Transportation Research Board*, 2220:66–74, May 2011.

D.A. Hausmann. Steel corrosion in concrete-how does it occur? *Materials Protection*, 6: 19–23, 1976.

M. Holz, S. Heil, and A. Sacco. A. temperature-dependent self-diffusion coefficients of water and six selected molecular liquids for calibration in accurate 1h nmr pfg measurements. *Physical Chemistry Chemical Physics*, 2:4740–4742, 2000.

David L. Jacobson, Daniel S. Hussey, E. Baltic, J. Larock, M. Arif, J. Gaglirg, J. Owejain, and T. Trabold. Neutron Radiography and Tomography Facilities at NIST to Analyze In-Situ PEM Fuel Cell Performance. *Neutron Radiography*. 50-57, 2008.

Scott Z. Jones, Nicos S. Martys, Yang Lu, and Dale P. Bentz. Simulation studies of methods to delay corrosion and increase service life for cracked concrete exposed to chlorides. *Cement and Concrete Composites*, 58:59–69, 2015.

W.D. Lindquist, D. Darwin, J. Browning, and G.G. Miller. Effect of cracking on chloride content in concrete bridge decks. *ACI Materials Journal*, 103:467–473, 2006.

R. Mills. *Self-diffusion in electrolyte solutions: a critical examination of data compiled from the literature*. Elsevier Science Pub. Co, 1989.

B.H. Oh, S.Y. Jang, and Y.S. Shin. Experimental investigation of the threshold chloride con- centration for corrosion initiation in reinforced concrete structures. *Magazine of Concrete Research*, 55:117–124, 2003.

R. Parthasarathy, A. Misra, J. Park, Q. Ye, and P. Spencer. Diffusion coefficients of water and leachable in methacrylate-based crosslinked polymers using absorption experiments. *Journal of Material Science: Material in Medicine*, 23:1157–1172, 2012.

P. Schiessl and W. Breit. Local repair measures at concrete structures damaged by reinforcement corrosion. aspects of durability. In *Proceedings of the* 4th *International Symposium" Corrosion of Reinforcement in Concrete Construction"*, pg525–534. The Royal Society of Chemistry, Cambridge, 1996.

Medhat H. Shehata, Michael D.A. Thomas, and Roland F. Blesznki. The effects of fly ash composition on the chemistry of pore solution in hydrated cement pastes. *Cement and Concrete Research*, 29:1914–20, 1999

Michael Thomas. Chloride thresholds in marine concrete. *Cement and Concrete Research*, 26:513 519, 1996.

L.A. Woolf. Isothermal diffusion measurements on the systems water-sodium chloride, water pentarerythritol, and water pentaerythritol-sodium chloride at 25°. *Journal of Physical Chemistry*, 67:273–277, 1963.